JOURNAL OF MATERIALS SCIENCE **36** (2001) 2773 – 2786

Characterization of close-celled cellular aluminum alloys

T. J. LU, J. M. ONG
Engineering Department, Cambridge University, Cambridge, CB2 1PZ, UK
E-mail: tjl21@eng.cam.ac.uk

The deformation behaviour of two different types of aluminium alloy foam are studied under tension, compression, shear and hydrostatic pressure. Foams having closed cells are processed via batch casting, whereas foams with semi-open cells are processed by negative pressure infiltration. The influence of relative foam density, cell structure and cell orientation on the stiffness and strength of foams is studied; the deformation mechanisms are analysed by using video imaging and SEM (scanning electronic microscope). The measured dependence of stiffness and strength upon relative foam density are compared with analytical predictions. The measured stress versus strain curves along different loading paths are compared with predictions from a phenomenological constitutive model. It is found that the deformations of both types of foams are dominated by cell wall bending, attributed to various process induced imperfections in the cellualr structure. The closed cell foam is found to be isotropic, whereas the semi-open cell foam shows strong anisotropy.

1. Introduction

Porous materials are found in a variety of microstructural forms, one of these has been termed as cellular. The most important feature of a cellular solid is its relative density, $\rho(\equiv \rho^*/\rho_s)$; that is, the density of the cellular material, ρ^*, divided by that of the solid from which the cell walls are made, ρ_s. The cellular geometry may be two dimensional, e.g. honeycombs, or three dimensional, e.g. foams. These materials are further classified into open and closed cell geometries. In open cell materials, the cells are interconnected such that there is a continuous pore phase throughout and the solid is an interconnected array of struts. Closed cell materials on the other hand, have a thin membrane of solid in the cell faces sealing them from neighbouring cells. If the foams are partly open and partly closed, it is said to be semi-open.

Cellular materials are widespread in everyday life and are known to have a high stiffness combined with very low specific weight [1]. For this reason foams are exploited in structural sandwich panel applications, where they are laminated between two dense materials as a means of maximising the moment of inertia with a minimal usage of material. Traditional cellular foams are mostly polymer or ceramic based. However, the processing of low cost metallic foams with a range of novel mechanical and physical properties has become possible due to recent developments in manufacturing methods [2]. The benefits of weight gaining and higher performance of metal foams, such as high stiffness [3], crash energy absorption [2], heat dissipation [4], non inflammability [5], noise control [6, 7], and corrosion resistance [2], have to be considered for the whole system to fully exploit the advantages of these advanced materials [8]. There is a growing literature on the mechanical-thermal-acoustic properties of metallic foams, see for example Gibson and Ashby [1] and Ashby *et al*. [2].

The present study aims at characterising the mechanical behaviour of two types of aluminium alloy foam, one with closed cells and the other with semi-open cells. Both foams have not been systematically studied before, especially when subjected to external loadings other than uniaxial tension and compression. The measured dependence of stiffness and strength on relative foam density will be compared to analytical predictions due to Gibson and Ashby [1]. In addition, the measured stress versus strain response will be compared to the predictions from the phenomenological constitutive model of Chen and Lu [9]. Deformation mechanisms for each type of foam will be studied using video imaging and SEM.

2. Theoretical considerations

2.1. Predicted properties of metallic foams

The properties of cellular materials can vary widely, depending on three main sets of parameters: the properties of the matrix material of which the cells are made, the apparent density and the structure of the cells. Other factors, which may also affect the properties, include temperature and anisotropy (cell orientation).

There are two basic architectures used to describe a foam: open cell and closed cell. Each structure results in different mechanical behaviour. Under uniaxial compression, open-celled foams deform by bending

followed, at sufficiently large loads, by the formation of plastic hinges within the cell walls. In closed cell foams, the deformation mechanism is more complicated. When a closed cell foam is deformed, bending of the cell edges is accompanied by stretching of the cell faces. For relative densities lower than 0.2, cell face stretching is the more significant mechanism of deformation in closed cell foams. However, imperfections present in metallic foams may change the picture dramatically [10].

By considering the mechanisms by which the cells deform and fail under uniaxial compression, the elastic modulus, E^*, and plastic collapse strength, $\sigma^*_{\rm pl}$ of cellular foams can be shown to depend upon the relative foam density by [2]

$$\frac{E^*}{E_{\rm s}} = \alpha_1 \left(\frac{\rho^*}{\rho_{\rm s}}\right)^n \tag{1}$$

$$\frac{\sigma^*_{\rm pl}}{\sigma_{\rm y}} = \alpha_2 \left(\frac{\rho^*}{\rho_{\rm s}}\right)^m \tag{2}$$

where $E_{\rm s}$ and $\sigma_{\rm y}$ denote the Young's modulus and yield strength of the solid wall material. Note that Equations 1 and 2 are the simplified versions of the property relations proposed by Gibson and Ashby [1]. For most metal foams, the material constants n has a value between 1.8 and 2.2, m between 1.5 and 2.0, α_1 between 0.1 and 4, and α_2 between 0.25 and 0.35, depending on the structure of the foam [2]. These predictions are true for metal foams having either closed or open cell structure. As with elastic collapse, large plastic strains in compression cause the cell walls to crush together. This results in a steep rise in the compressive stress versus strain curve when the applied strain exceeds a nominal compressive strain, known as the densification strain, $\varepsilon_{\rm d}$. The strain boundary defining the start of densification is given by:

$$\varepsilon_{\rm d} = 1 - \alpha_3 \left(\frac{\rho^*}{\rho_{\rm s}}\right) \tag{3}$$

where the material constant α_3 is about 1.4 for non-metallic foams [1] and between 1.4 and 2 for the currently available metallic foams [2]. Obviously the strain at which densification starts decreases as the relative density increases.

The mechanism of deformation during uniaxial tensile stressing can be described by a simple adaptation of Equations 1 and 2. The tensile modulus is not the same as that in compression, due to different deformation mechanisms [1, 2]; the tensile modulus is greater, typically by 10%. The tensile strength is about 1.1 to 1.4 times the compressive strength.

The shear deformation of cellular foams may be modelled by considering the bending, buckling and fracture of an idealised cell structure, i.e., regular hexagonal honeycombs [1]. The shear modulus G^* of the foam is then found to scale with the relative foam density as:

$$\frac{G^*}{G_{\rm s}} = (3/8)\alpha_1 \left(\frac{\rho^*}{\rho_{\rm s}}\right)^n \tag{4}$$

If shear modulus of the cell wall material can be calculated from: $G_{\rm s} = E_{\rm s}/2(1+\upsilon_{\rm s})$, where $\upsilon_{\rm s}$ is the Poisson ratio of the cell wall material, it then follows that

$$G^* \cong (3/8)E^* \tag{5}$$

However, if the Poisson ratio υ^* of a metal foam is different from $\upsilon_{\rm s}$ (see Equation 26 later), then (5) needs to be modified.

The failure analysis of foams when subjected to multiaxial stressing is more complicated than that for their uniaxial behaviour. Several collapse mechanisms can act simultaneously, but the mechanism that gives the lowest strength dominates the failure. For the case of a perfect 2-D honeycomb with regular hexagonal cells, the macroscopic bulk modulus K^* and hydrostatic strength $\sigma_{\rm h}$ are given by [1]

$$\frac{K^*}{E_{\rm s}} = 0.25\left(\frac{\rho^*}{\rho_{\rm s}}\right), \quad \frac{\sigma_{\rm h}}{\sigma_{\rm y}} = 0.5\left(\frac{\rho^*}{\rho_{\rm s}}\right) \tag{6a}$$

which are typically an order of magnitude larger than the Young's modulus and uniaxial compressive strength of the honeycomb, see Equations 1 and 2. This is due mainly to the difference in deformation mechanisms, with cell wall stretching dominating in hydrostatic compression and cell wall bending dominant under uniaxial stressing. However, it has been established that the presence of a small degree of geometrical imperfections in the cellular structure will easily trigger cell wall bending under arbitrary loading, and hence significantly reduce the stiffness and strength of the honeycomb under hydrostatic stressing to a level comparable to that of the corresponding uniaxial properties [10]. For 2D foams having imperfect cellular structures (e.g., fractured cell walls), it is found from finite element analysis that [10]

$$\frac{K^*}{E_{\rm s}} = \alpha_4 \left(\frac{\rho^*}{\rho_{\rm s}}\right)^3, \quad \frac{\sigma_{\rm h}}{\sigma_y} = \alpha_5 \left(\frac{\rho^*}{\rho_{\rm s}}\right)^2 \tag{6b}$$

where $\alpha_4 \approx 1$ and $\alpha_5 \approx 0.4$. For metallic foams, Equation 6b is consistent with experimental measurements, whereas Equation 6a is not [2, 10, 11].

2.2. Constitutive modelling

Under stressing, metallic foams are elastic-plastic and exhibit strongly pressure sensitive yielding behaviour. Several constitutive models have been proposed to describe the yielding of foams. Using a mechanism-based micromechanics model for open-celled rigid polymeric foams, Gibson *et al.* [12] derived a yield surface

$$\frac{\sigma_{\rm e}}{\sigma_{\rm s}} = \pm\lambda\rho^{-3/2}\left[1 - \left(\frac{3\sigma_{\rm m}}{\sigma_{\rm s}\rho}\right)^2\right] \tag{7}$$

where λ is a material constant to be evaluated by uniaxial loading, and $\sigma_{\rm e}$, $\sigma_{\rm m}$ are the Mises effective stress

and mean stress, respectively, given by

$$\sigma_e = \sqrt{\frac{1}{2}\left[(\sigma_1-\sigma_2)^2+(\sigma_2-\sigma_3)^2+(\sigma_3-\sigma_1)^2\right]}$$

$$\sigma_m = \frac{\sigma_1+\sigma_2+\sigma_3}{3} \tag{8}$$

where σ_i $(i=1,2,3)$ are the principal stresses. However, due to the complicated failure mechanisms associated with the irregular and imperfection-prone microstructures commonly found in foams, it is difficult to derive user-friendly yield functions from micromechanics study. A phenomenological approach has therefore been widely applied to formulate the constitutive model for both polymeric and metallic foams. The analytical results of Gibson *et al*. are fitted by Puso and Govindjee [13] with a single elliptical yield surface given, in the σ_e–σ_m space, by

$$\sigma_e^2 + \frac{1}{R}\sigma_m^2 - h^2 = 0 \tag{9}$$

where R and h are material parameters. This model is extended by Zhang *et al*. [14] to study the yielding of polymeric foams, with an added parameter to define the centre of the yield locus,

$$\frac{[\sigma_m - X_0(\varepsilon_{mp})]^2}{a(\varepsilon_{mp})} + \frac{\sigma_e^2}{b(\varepsilon_{mp})} \le 1 \tag{10}$$

where ε_{mp} is the plastic volumetric strain, and $X_0(\varepsilon_{mp})$, $a(\varepsilon_{mp})$, $b(\varepsilon_{mp})$ are material parameters to be determined from uniaxial compression, simple shear, and hydrostatic compression tests.

Compared with rigid polymeric foams, the yielding of metal foams is complicated by the presence of various types of morphology imperfections [10]. Whilst Equation 7 suggests that the hydrostatic yield strength of a perfect foam is governed by cell wall stretching and that its uniaxial strength is dominated by cell wall bending, Chen *et al*. [10] found that a small degree of imperfections such as cell wall waviness and misalignment suffices to induce cell wall bending under all macroscopic stress states, reducing the hydrostatic strength to the same level as the uniaxial strength. Based upon the elliptical yield function (9), Deshpande and Fleck [11] proposed two phenomenological constitutive models for metallic foams: the self-similar model and the differential hardening model. In the first model, the aspect ratio R of the ellipse is a material constant while h depends not only upon the accumulated plastic strain but also upon the stress state and is characterised by the uniaxial and hydrostatic compression stress versus strain curves. The more complicated differential hardening model is developed to capture the experimentally observed evolution of shape of yield surface in metallic foams. Here, both R and h are assumed to be strain *and* stress states dependent, requiring four material parameters to characterise hardening. Although improved accuracy is obtained by using the differential hardening model, detailed test data on the initial yield surface and its evolution must be provided to determine the four material parameters.

Recently, Chen and Lu [9] established a unified framework of constructing phenomenological constitutive models for a broad class of elasto-plastic materials exhibiting either plastical incompressibility (e.g., grey cast iron) or plastical compressibility (e.g., metal foams). The constitutive framework also enables the different yielding behaviours under tension and compression as well as differential hardening along different loading paths to be accounted for in a relatively simple manner. The resulting plasticity model does not require the difficult task of experimentally probing the initial yield surface and its subsequent evolution—it is completely determined from a set of as few as two distinctive stress versus strain curves measured along characteristic loading paths. In this general framework, a characteristic stress $\bar{\sigma}$ and its work conjugate $\bar{\varepsilon}$, the characteristic strain, are introduced as

$$\bar{\sigma} = \left(\sigma_e^2 + \beta^2\sigma_m^2\right)^{1/2} \tag{11}$$

$$\bar{\varepsilon} = \left(\varepsilon_e^2 + \frac{\varepsilon_v^2}{\beta^2}\right)^{1/2} \tag{12}$$

where β is a parameter related to the Poisson ratio of the material by

$$\beta = \left[\frac{9(1-2v)}{2(1+v)}\right]^{1/2} \tag{13}$$

Note that, with the introduction of $\bar{\sigma}$ and $\bar{\varepsilon}$, the elastic complementary energy, W, can be separated into the distortional and volumetric parts, as

$$W = \frac{1}{2\bar{E}}\left[\sigma_e^2 + \beta^2\sigma_m^2\right] \tag{14}$$

where $\bar{E} = 3E/2(1+v)$. A yield function in terms of $\bar{\sigma}$ and $\bar{\varepsilon}$ is then proposed as

$$\Phi = \bar{\sigma}^2 + C(\bar{\varepsilon})\sigma_m^2 - Y(\bar{\varepsilon}) = 0 \tag{15}$$

where $C(\bar{\varepsilon})$ and $Y(\bar{\varepsilon})$ are material properties to be evaluated by two characteristic tests: in the present study, uniaxial compression and hydrostatic compression tests will be used. It is proposed to use Φ in conjunction with the associated flow rule to calculate the *total* strain rate as

$$\dot{\varepsilon}Y'_{ij} = \dot{\lambda}Y'\frac{\partial\Phi}{\sigma_{ij}} \tag{16}$$

where the proportionality factor $\dot{\lambda}$ is determined from the consistence condition of plasticity as

$$\dot{\Phi} = \frac{\partial\Phi}{\partial\sigma_{ij}}\dot{\sigma}_{ij} + \frac{\partial\Phi}{\partial\bar{\varepsilon}}\dot{\bar{\varepsilon}} = 0 \tag{17}$$

From the measured stress versus strain curves under uniaxial compression and hydrostatic compression, the

two material parameters $C(\bar{\varepsilon})$ and $Y(\bar{\varepsilon})$ can be easily determined as

$$C(\bar{\varepsilon}) = \frac{\bar{\sigma}_{hc}^2 - \bar{\sigma}_{uc}^2}{\bar{\sigma}_{uc}^2/(9+\beta^2) - \bar{\sigma}_{hc}^2/\beta^2}$$
$$Y(\bar{\varepsilon}) = \bar{\sigma}_{hc}^2 \bar{\sigma}_{uc}^2 \frac{1/(9+\beta^2) - 1/\beta^2}{\bar{\sigma}_{uc}^2/(9+\beta^2) - \bar{\sigma}_{hc}^2/\beta^2} \quad (18)$$

where the subscripts 'uc' and 'hc' used to denote uniaxial compression and hydrostatic compression, respectively. Together with the associated flow rule (16) and consistence condition (17), the yield function (15) can now be used to study the constitutive behaviours of foams having either closed or open cells. Stress versus strain curves under several different proportional loading paths are reported in detail by Deshpande and Fleck [11] for a high density closed cell aluminium foam (Alporas foam from Shinko Wire Company, Japan) and for a low density open cell aluminium foam (Duocel foam from ERG Company, USA). Close agreement between the model predictions and the experimental measurements of Deshpande and Fleck [11] has been reported by Chen and Lu [9].

3. Preparation of materials

Two types of aluminium foams are examined in this study, all made by a foam casting method, but with distinctly different foaming strategies. Both materials, processed at the Southeast University, China with a range of relative densities, will be called below the SEU foams. For convenience, the semi-open foams with relative densities of 0.39 and 0.35 are labelled Sample 1 and 2 respectively. Similarly, the closed cell foams are named Samples 3, 4, 5 and 6, with Sample 3 having the highest relative density of the four. For each sample, its bulk density, relative density and the type of tests performed are summarised in Table I. At least two specimens are prepared and tested for each type of sample. The material axes of the SEU foams are defined such that the X_2-axis is parallel to the foaming direction and the X_1-axis is perpendicular to foaming direction, as shown in Fig. 1b. All samples were loaded in the X_1 direction unless otherwise specified. All samples were cut to size using the electric discharge machine (EDM) to minimise local cell wall damage.

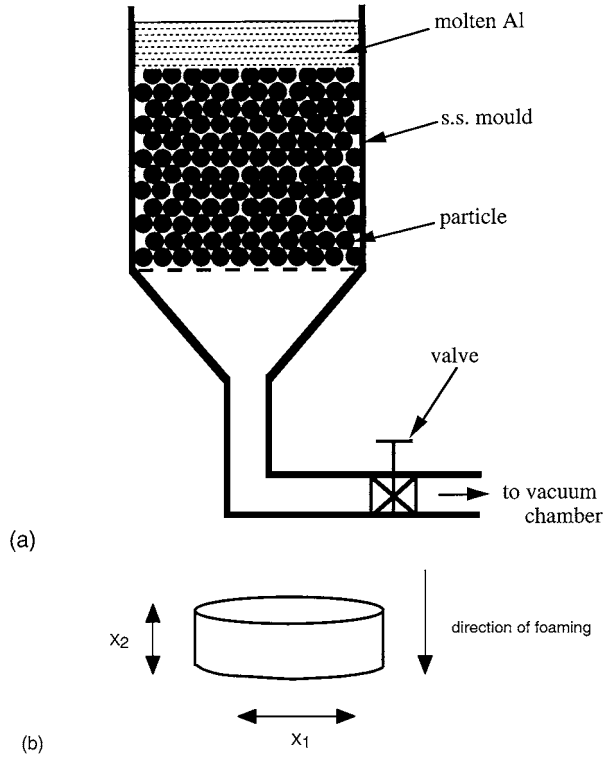

Figure 1 (a) Processing of semi-open cell SEU foams with the negative infiltration method, (b) definition of material axes for SEU foams, with X_1 and X_2-axes perpendicular and parallel to the foaming direction, respectively.

3.1. Semi-open foams

The SEU semi-open aluminium alloy foams are made via the negative pressure infiltration method, where an interconnected cellular structure (i.e., sponge metal) may be obtained by infiltrating a bed of spherical particulates with a liquid aluminium alloy melt. This technique incorporates the benefits of net-shape production of cellular aluminium parts and integral-casting of dense and porous parts.

Spherical particles are made by a specially designed machine which mixes very fine Al_2O_3 powders with a binder solution—composed of inorganic salt (e.g., Na_2CO_3) and water—to form round particles and 'roll' these particles until they become (approximately) spherical. The selection of fine Al_2O_3 powder is based on its high temperature resistance, excellent removability after foaming, good formability, high stiffness

TABLE I Physical and mechanical properties of SEU metal foams

Sample	1	2	3	4	5	6
Bulk density (g/cm^3)	1.07	0.95	0.45	0.43	0.38	0.30
Relative density	0.39	0.35	0.17	0.16	0.14	0.11
Cell morphology	Semi-open	Semi-open	Closed	Closed	Closed	Closed
Compression						
Young's modulus (GPa)*						
–Loading	2.94	2.47	1.04	0.82	0.74	0.60
–Unloading	3.00	2.72	1.23	1.10	0.83	0.67
Strength (MPa)*	18.85	19.21	5.47	4.37	3.88	2.34
Shear						
Modulus (GPa)*			0.65	0.56	0.44	0.36
Strength (MPa)*			3.22	2.53	2.26	1.54

*Error of measurement = 10–15%.

and strength, low thermal conductivity, and, most importantly, non-wettability with molten aluminium alloy. After baking (in order to make the inorganic salt crystallise), the particles are separated, via screening, into groups with varying sizes: 0.3–0.45, 0.45–0.6, 0.6–1.0, 1.0–1.25, 1.25–1.6 mm, with those obviously less spherical discarded. The particles from a selected group are randomly packed, assisted by mechanical vibration, into a cylindrical stainless steel mould of diameter 200 mm. The mould is then preheated in a specially designed oven, maintained at 700°C for about 30 minutes to ensure uniform heating of the particles. Molten aluminium of temperature ~720°C is subsequently infiltrated into the preform under controlled pressure (Fig. 1a). After the mould cools down to room temperature, the particle/Al composite is removed; the particles are then separated from the Al skeleton and washed away by an water jet. In addition to pure Al, the casting alloy comprises about 6.5–7.5% Si and 0.25–0.45% Mg. The aluminium alloy has a density of 2.68 Mg/m^3 and melting temperature of 615°C.

3.2. Closed cell foams

The SEU closed cell aluminium alloy foam is produced by a method better known as the batch casting process. The relatively short time interval between adding a foaming agent to the molten alloy and foam formation makes the casting operation difficult. The key is to control the viscosity of the melt. With low viscosity, the bubbles float easily to the surface and gas is dissipated into atmosphere. On the other hand, if viscosity is too high, bubbles hardly float in the foaming molten material and gas pressure rises so high in the centre of the molten material that the cell collapses. Thickening is one means of enabling the foamed metal to be maintained in its heated, fluid condition for relatively prolonged periods without collapsing. In foams produced by thickening method followed by foaming the pore size is smaller and more uniform.

To process the SEU closed cell foams, foaming agent titanium hydride (TiH_2) is added to the molten metal. When heated to a temperature above 465°C, it decomposes into Ti and gaseous H_2. As a result, large volumes of hydrogen gas are produced, creating bubbles that can lead to a closed cell foam, provided foam drainage is sufficiently slow, requiring a relatively high melt viscosity. The process begins by melting aluminium and stabilising the melt temperature between 670 and 690 C. Its viscosity is then raised by adding 1–2% of calcium which rapidly oxidises and forms finely dispersed CaO and $CaAl_2O_4$ particles. The melt is aggressively stirred and 1–2% of TiH_2 is added. Once the foam expands to the desired volume, the melt is cooled to solidify the foam before the hydrogen escapes and the bubbles coalesce or collapse.

4. Experimental procedures

4.1. Uniaxial compression

Uniaxial compression tests were carried out on closed cell and semi-open cell foam specimens using the servo hydraulic Instron 8872 testing machine with a maximum load capacity of 25 kN. The cuboid samples, each of dimensions $20 \times 20 \times 40$ mm, were loaded in the X_1 direction. Additional samples were also tested in the X_2 direction to investigate the degree of anisotropy. Compression testing was performed at a crosshead rate of 2 mm/min, and was carried out to a total deformation of 75% whenever possible. The deformation of the cellular material was determined from the crosshead displacement of the machine. Loading and unloading of the stress versus strain curve was repeated at different stages of the deformation throughout the test. The elastic behaviour is characterised by a stiffness parameter, E, determined from the unloading portion of an unload-load cycle early in the test. The two parallel loading platens were coated with a PTFE spray to reduce friction between the specimen and loading platens.

The compressive strength of a closed cell SEU foam is taken as the yield strength measured at a nominal strain of 10%. The compressive strength of a semi-open cell SEU foam is defined by the 2% proof stress, as its stress versus strain curve is different from that corresponding to a closed cell sample, with strong hardening observed in one loading direction and weak hardening in the other (see Fig. 7 later).

4.2. Uniaxial tension

Uniaxial tensile tests were performed with an Instron testing machine—Model 5530R—by using the 10 kN load cell and a clip gauge attached to the reduced central region of the specimen. All specimens had a rectangular, dogbone shape geometry; the overall dimensions are 150 mm long, 30 mm wide and 20 mm thick. The specimens contained a waisted region 40 mm in length and 20×15 mm in cross section. This region acts to localise the deformation and to prevent premature failure in the grip sections. These specimens were then loaded in the X_1 direction at a rate of 0.5 mm/min.

Special care was undertaken to ensure that the standard Instron grips which were used to transmit the load applied by the testing machine to the specimen were tighten sufficiently to avoid slip of the specimen, but not excessively to the extent of crushing the material as this would introduce undesirable bending stresses. Misalignment in the grips could cause significant elastic bending stresses that superimpose on uniaxial stresses. This may cause localised microplastic flow and localised rupture at lower applied stresses than the true average uniaxial tensile stress typically required.

4.3. Simple shear

The shear properties were investigated by means of a double lap shear test, using a specimen consisting of two rectangular test samples of dimensions $100 \times 20 \times 20$ mm sandwiched between three steel load plates (Fig. 2). The samples were bonded to the steel plates using epoxy REDUX 325, and left for at least 24 hours before carrying out the tests on the Instron 5530R testing machine with a 100 kN load cell. Only the closed cell foams were tested in simple shear, due

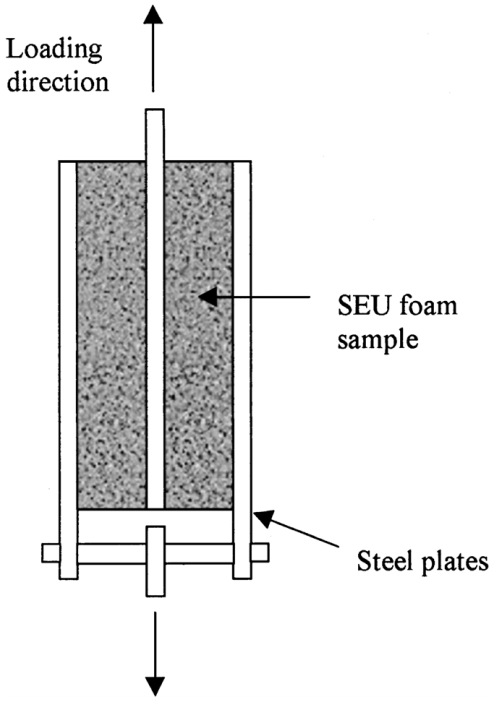

Figure 2 Geometry of double shear lap specimen.

partly to the anisotropy exhibited by the semi-open cell foams and partly to the difficulty of preventing interfacial debonding failure between the semi-open cell foam and the loading plates.

The relative displacement between the loading plates was measured using a clip gauge. It is attached to the middle load plate and the side plates, and measures the position of the middle plate relative to the side plates during loading. A tensile load was applied to the ends of the load plates through a universal joint so as to distribute the load uniformly across the width of the specimen. Based on preliminary test results, the load was applied using a constant crosshead speed of 0.5 mm/min in order to reach the maximum loads within 3 to 6 minutes as recommended by the ASTM standard. The stress corresponding to the maximum load is taken as the shear strength of the foam. The shear modulus is calculated from the slope of the shear stress versus shear strain curve in the linear-elastic region.

4.4. Hydrostatic compression

The multiaxial compression tests were carried out on a closed cell SEU foam (Sample 5) using a high-pressure triaxial loading system which was developed originally for studying powder compaction and adapted later to probe the yield surface of Alporas and ERG foams [11]. It consists of a pressure chamber and a piston rod for the application of axial force. Hydraulic fluid is used as the pressurising medium, and the pressure chamber is designed to withstand a maximum pressure of 100 MPa. Cylindrical specimens of diameter 30 mm and length 40 mm were tested.

During the hydrostatic compression tests, the confining pressure was increased in increments of 0.1 MPa and the corresponding change in volume of the specimen was deduced from the axial displacement. When the SEU foam is subjected to hydrostatic pressure, both compressive radial and axial strains were induced. The decrease in axial length of the cylindrical specimen was measured using a linear variable displacement transducer (LVDT) attached to the triaxial cell. With the assumption that the closed cell SEU foam deforms in an isotropic manner (which is confirmed later, see below), the volumetric strain is equal to three times the axial strain. There is no provision in the present triaxial cell design for measuring the change in diameter of the foam sample during hydrostatic loading. Therefore, it is not suitable for samples that show signs of anisotropy, as is the case of semi-open SEU foams. Note that in all these experiments, the error of measurement is typically on the order of 10–15%.

5. Results and discussion

5.1. Uniaxial compression

Uniaxial compressive stress versus strain curves for SEU foams having different relative densities are plotted in Fig. 3; all samples are loaded along the X_1 direction. The curves show that, as the relative density decreases, the Young's modulus, plastic collapse strength, and slope of the stress versus strain curve through the plastic collapse region all decrease, while the strain at which densification begins increases. In Fig. 4a, the measured compressive strength σ^*_{pl} of closed cell SEU foams is plotted against relative foam density ρ; the result can be described by a fractional power relationship, given by

$$\frac{\sigma^*_{\text{pl}}}{\sigma_{\text{y}}} = 0.98\left(\frac{\rho^*}{\rho_{\text{s}}}\right)^{1.5} \tag{19}$$

For comparison purposes, the compressive stress in each curve has been normalised by the plastic collapse stress σ_{y} of the solid material. Whilst the power index $m = 1.5$ is consistent with that for other types of closed cell foams, the proportionality coefficient α_2 has a slightly higher value of 0.98. The elastic modulus E^* of closed cell SEU foams measured from the first few hysteresis loops is presented in Fig. 4b as a function

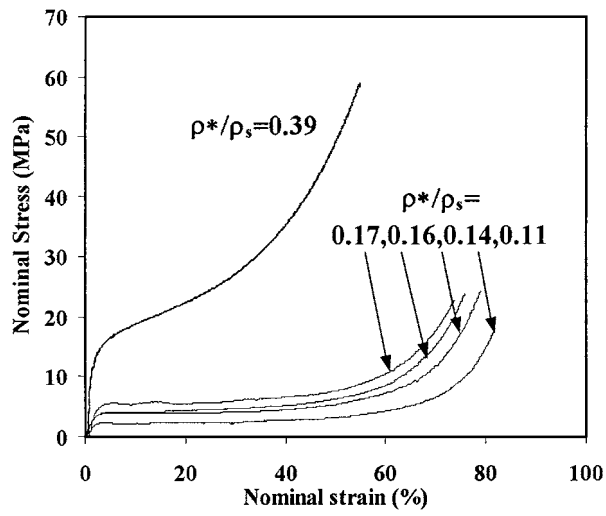

Figure 3 Uniaxial compressive stress versus strain curves of SEU foams of various relative densities.

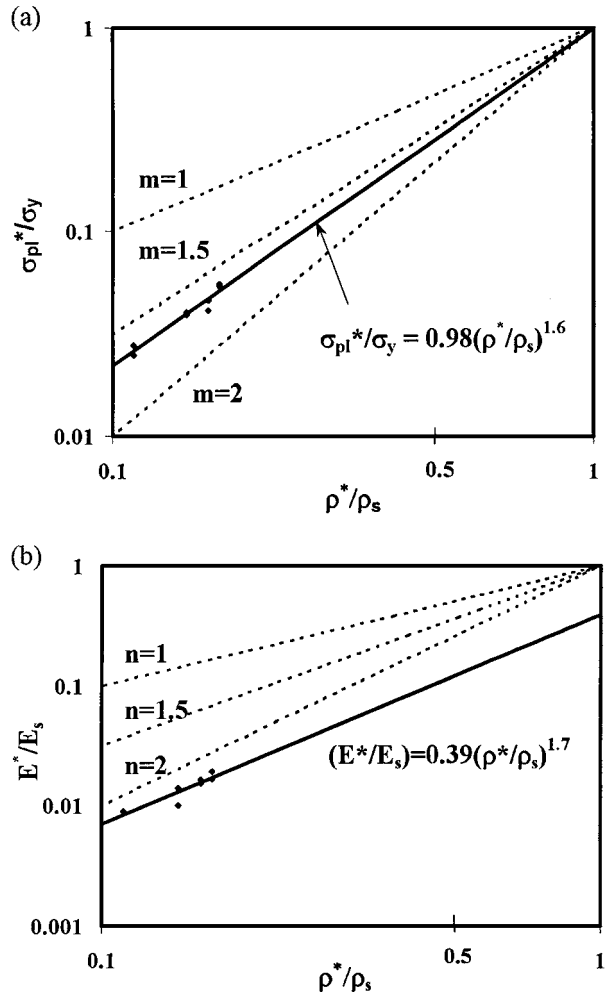

Figure 4 (a) Compressive strength, (b) Young's modulus of SEU closed cell foams as functions of relative foam density. The dotted lines are predictions by Equations 1 and 2, and the full line is a best fit for experimental results.

of ρ. The experimental data are consistent with those predicted by (1), with

$$\frac{E^*}{E_s} = 0.4\left(\frac{\rho^*}{\rho_s}\right)^{1.7} \tag{20}$$

Note that the exponent of Equation 20 is slightly different from that proposed in [1]. This may be caused by experimental error, or because the model used in [1] is for foams having idealized pore morphologies, or a combination of both. The elastic modulus E^* of the SEU foams is not constant but varies as the applied strain is increased. Fig. 5 presents E^* of a closed cell SEU foam ($\rho = 0.11$) as a function of compressive strain; the corresponding stress versus strain curve is also included in Fig. 5 for comparison. The much smaller elastic modulus of the foam upon initial loading is believed to result from immediate yielding at cell nodes due to stress concentration [15], and hence has been ignored in Fig. 5. It is seen from Fig. 5 that E^* initially decreases with increasing strain by as much as 20–50%, reaching a minimum at a strain of about 20–25%, and then increases due to densification. The relatively large drop in E^* during the initial stage of compression is attributable to the fracturing of cell faces

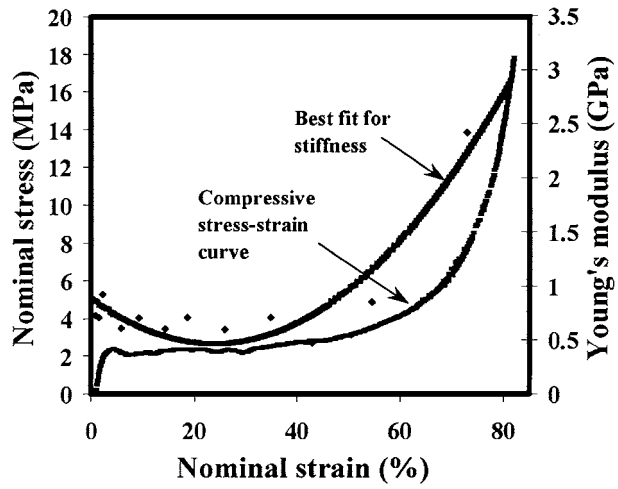

Figure 5 Young's modulus plotted as a function of nominal strain for a closed cell SEU foam of relative density 0.11. A polynomial to the power of 5 is used to fit for $E(\varepsilon)$.

as well as geometrical softening due to cell wall bending; similar behaviour has been reported for other types of aluminium alloy foam [6].

The deformation development in the closed cell SEU foam of relative density 0.11 at different stages of compressive strain is illustrated in Fig. 6. After the initiation of plastic collapse, there are both deformed and undeformed regions in the cellular structure, i.e., complete collapse of some parts has occurred while the rest is still elastic. Therefore, two strain states coexist at almost the same stress. In most specimens, plastic collapse initiates from within a localised band at roughly mid-height of the specimen. The collapse bands increase in size with increasing strain until the whole specimen collapses. Pore collapse occurs essentially by plastic yielding of the cell walls throughout the entire deformation bands, and yielding appears in a layer roughly perpendicular to the direction of compressive stress. Some foam samples exhibited multiple secondary deformation bands throughout the specimen rather than a single dominant band. Progressive collapse was marked by both the expansion of existing deformation bands and the formation of new ones. The load resistance of the closed cell foam sample remained fairly constant after cell collapse, increasing only slightly in some cases, see Fig. 3. The rate of increase became larger as the specimen approached densification.

To check the effect of cell orientation (relative to the foaming direction) on stiffness and strength, selected samples of SEU foams with closed cells were also tested under uniaxial compression in the X_2 direction. Fig. 7a compares the measured compressive stress versus strain curve for a sample of relative density 0.14 loaded in the X_2 direction with that in the X_1 direction. It is clear from Fig. 7a that the material exhibits (nearly) isotropic behaviour; the deformation mechanisms observed are also similar for both cases. Similar trends have been observed for closed cell SEU foams with different relative densities. The same tests were also carried out for the semi-open cell SEU foam of relative density 0.35; the corresponding stress versus strain curves are presented in Fig. 7b. Clearly, the semi-open

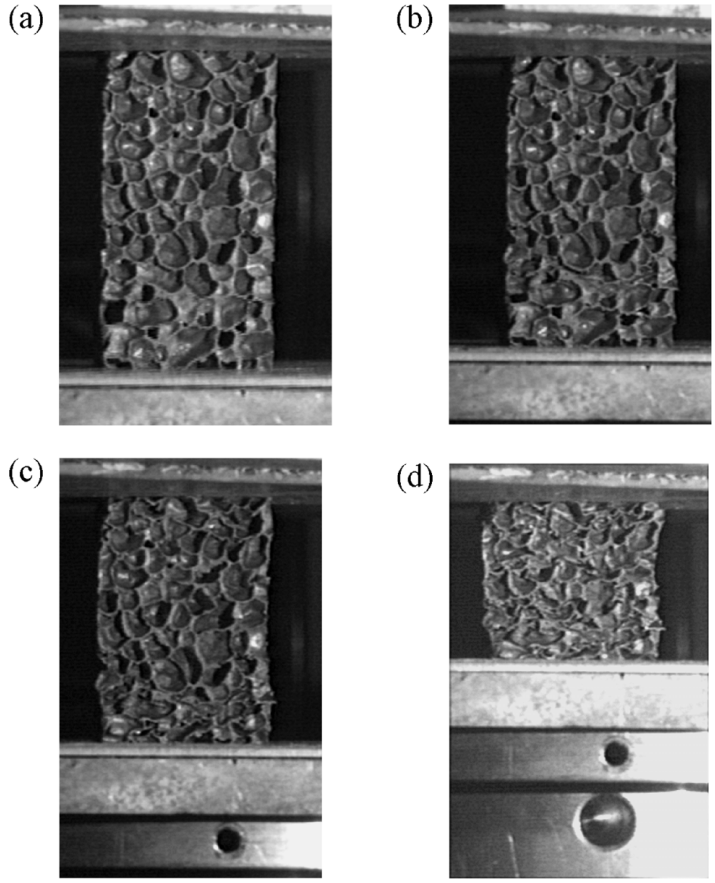

Figure 6 Deformation of closed cell SEU sample ($\rho = 0.11$) at various stages of uniaxial compression, corresponding to (a) 0%, (b) 10%, (c) 25%, (d) 50% of applied strain.

cell foam is strongly anisotropic. When loaded in the X_1 direction, multiple deformation bands were formed in semi-open cell foams before eventually reaching densification (Fig. 8a), which is somewhat similar to that observed for the closed cell foams. However, whilst the closed cell foams have weak strain hardening, the semi-open cell foams exhibit strong strain hardening behaviour (Fig. 7b). This may be caused by the relatively large relative density of the semi-open cell foam tested ($\rho = 0.35$), in comparison to the highly porous closed cell foams ($\rho \approx 0.1$). On the other hand, when loading was applied to the semi-open cell foam specimen ($\rho = 0.35$) along the foaming direction, X_2, a totally different deformation mechanism occurs (Fig. 8b). Here, multiple shear bands form and, as the compression test proceeds, the sample crumbles at relative low strain levels ($\sim$30%) due to the formation of relatively large cracks in the direction of loading. The corresponding stress versus strain curve (Fig. 7b) shows initially linear elastic behaviour at small strains, followed by a plastic yielding region where multiple shear bands form before decreasing rapidly once crumbling takes place. This is further confirmed when the semi-open foam sample is analysed using the SEM (Fig. 9). The foam sample exhibits a visually discernible gradient in cell size, shape and orientation across the X_1 and X_2 planes as defined in Fig. 1b, due to the geometric constraints on the foam during infiltration processing. In the transverse direction, X_1, the cells are mostly rounded with small variation in size and shape across the surface (Fig. 9a). However, in the longitudinal direction, X_2, it was found that the cell orientation is nearly vertical, parallel to the foaming direction X_2, and the cells are ellipsoidal-shaped, with a wider cell size variations (Fig. 9b). The degree of anisotropy may be measured by the ratio of the strength in the transverse direction to that in the longitudinal direction. Hence, from the results shown in Fig. 7, the semi-open cell foams have a degree of anisotropy of about 1.72 and the closed cell foams about 1.02. In comparison, Alporas and ERG foams are isotropic, whereas the Alulight foam produced by Mepura Ltd., Austria, has a degree of anisotropy of about 1.33 [16].

The Young's modulus and plastic collapse strength of SEU aluminium alloy foams normalised by those of the solid aluminium are plotted against relative density, ρ^*/ρ_s in Fig. 10a and b, respectively, and are compared with those of commercially available aluminium alloy foams. More detailed results are summarised in Table I. These provide useful information to a design engineer in the material selection process.

5.2. Uniaxial tension

Typical uniaxial tensile stress versus strain curves are shown in Fig. 11a for different relative densities of the SEU foams having either closed or semi-open cells. The curves show linear elastic behaviour at small strains ($<$2%), followed by yielding and strain hardening up to the peak stress, whereupon the load decreases rapidly

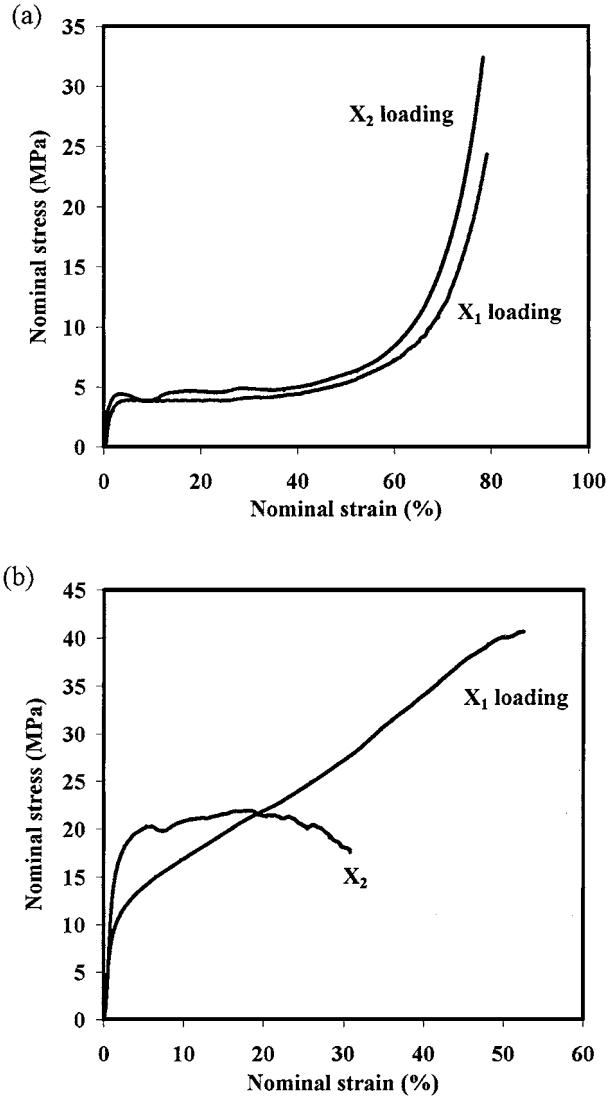

Figure 7 Comparison of uniaxial compressive stress versus strain curves X_1 and X_2 directions for (a) closed cell SEU foam ($\rho = 0.14$), (b) semi-open foam ($\rho = 0.35$).

due to cracking. The linear elastic part of the curve signifies linear-elastic elongation behaviour; the straightening of curved cell edges or walls, where the elongation of the cells are in the direction parallel to the tensile load applied, seems to be predominating. After a short plastic elongation a crack initiates and extends to cut across the foam core. When the peak load is reached, many specimens bent (as a result of stable crack propagation) before finally necking and subsequent rupturing, preventing accurate measurement of the ultimate strain.

The tensile strength of closed cell SEU foams are plotted against relative density in Fig. 11b; the Young's modulus obtained in the tensile test has a value similar to that of the compressive elastic modulus, and hence are not reported below. When the data are fitted by using Equation 2, the value of the index m is found to be approximately 2. With increasing relative density, the tensile strength increases and the strain at which the peak strength is measured decreases. For example, Sample 3 with relative density of 0.17 reaches its peak strength at a strain of 4.1%, whereas Sample 6 having a lower relative density of 0.11 peaks at a strain of about 2.75%.

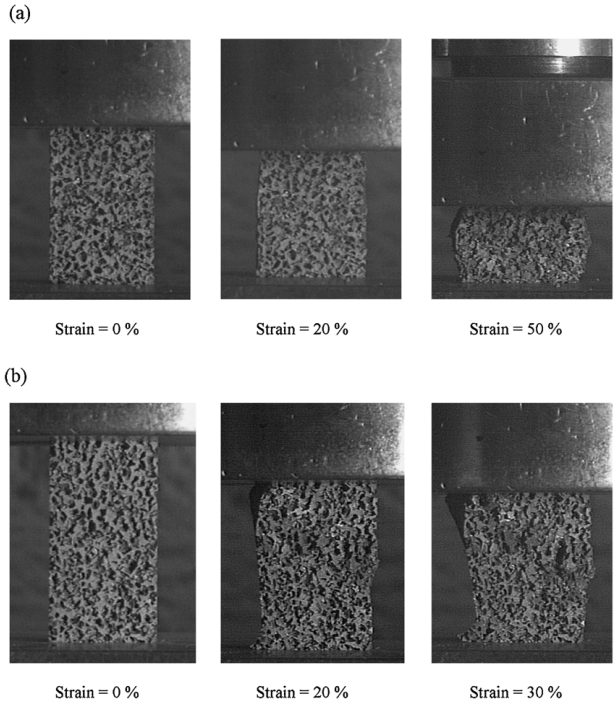

Figure 8 Video images of progressive deformation and failure of semi-open SEU foam ($\rho = 0.35$) when loaded along (a) X_1, (b) X_2 directions.

The tensile strength of closed cell SEU foams is significantly lower than their compressive strength listed in Table I. It appears that the tensile test is especially critical to inhomogeneities of the foam samples. This may be explained by the voids or cracks present in the material as a result of differential thermal contraction during processing of foamed aluminium, which appears to be more harmful in tension than in compression.

5.3. Shear

Shear stress versus strain curves for closed cell SEU foams with different relative densities are shown in Fig. 12. Each curve demonstrates an almost linear-elastic beginning that changes gradually into plastic deformation. Elongation of cell walls similar to that in the tensile test was observed during the earlier part of the shear test. When the maximum shear load is reached, failure is visible as a crack is seen to run across the whole sample. A fast failure was observed after the maximum load is reached, similar to that observed during the tensile test. In all these tests, failure initiated from the foam core, instead of from the foam/plate interface.

The shear test results are summarised in Table I. Fig. 13a and b illustrate the effect of relative density on the shear moduli and shear strength of closed cell SEU foams; the experimental data were found to be closely described by the following power-law type relationships

$$\frac{G^*}{G_s} = 0.27\left(\frac{\rho^*}{\rho_s}\right)^{1.4} \tag{21}$$

$$\frac{\tau^*}{\tau_s} = 1.04\left(\frac{\rho^*}{\rho_s}\right)^{1.6} \tag{22}$$

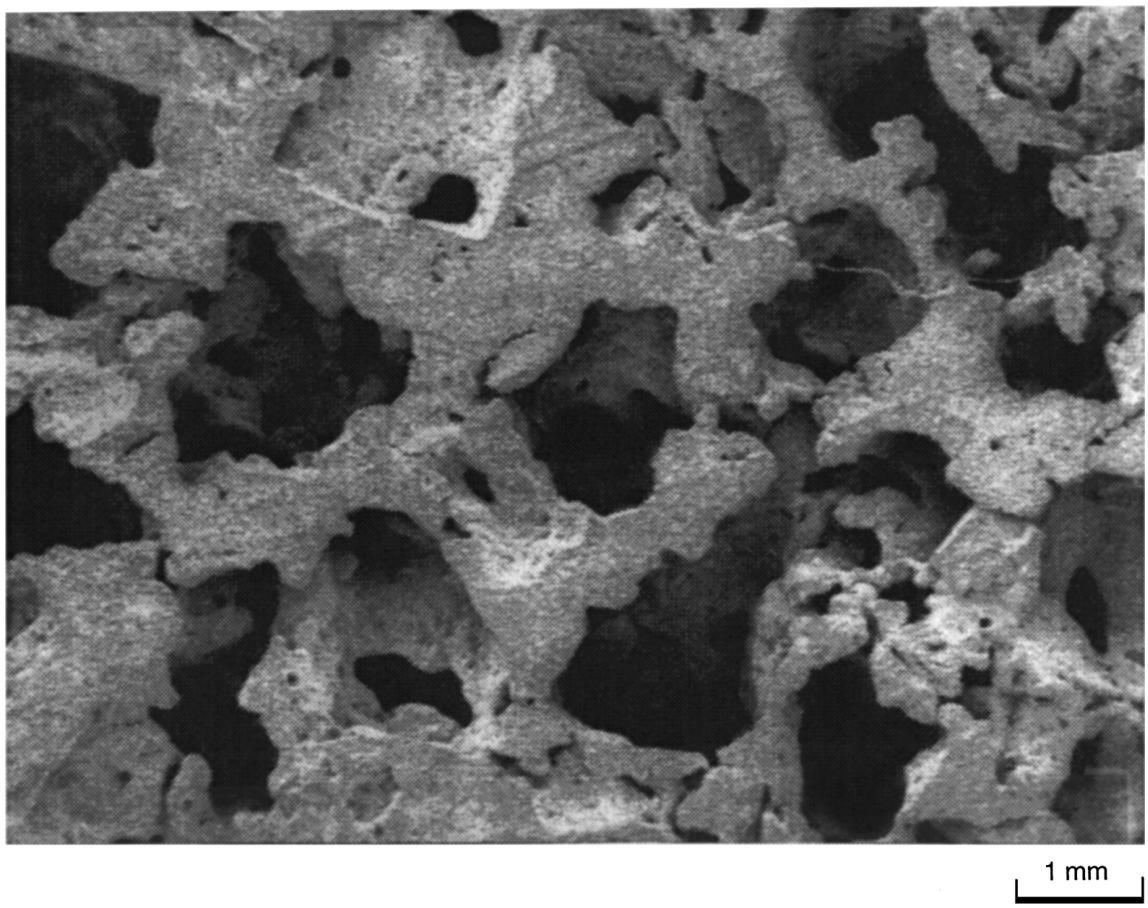

(a)

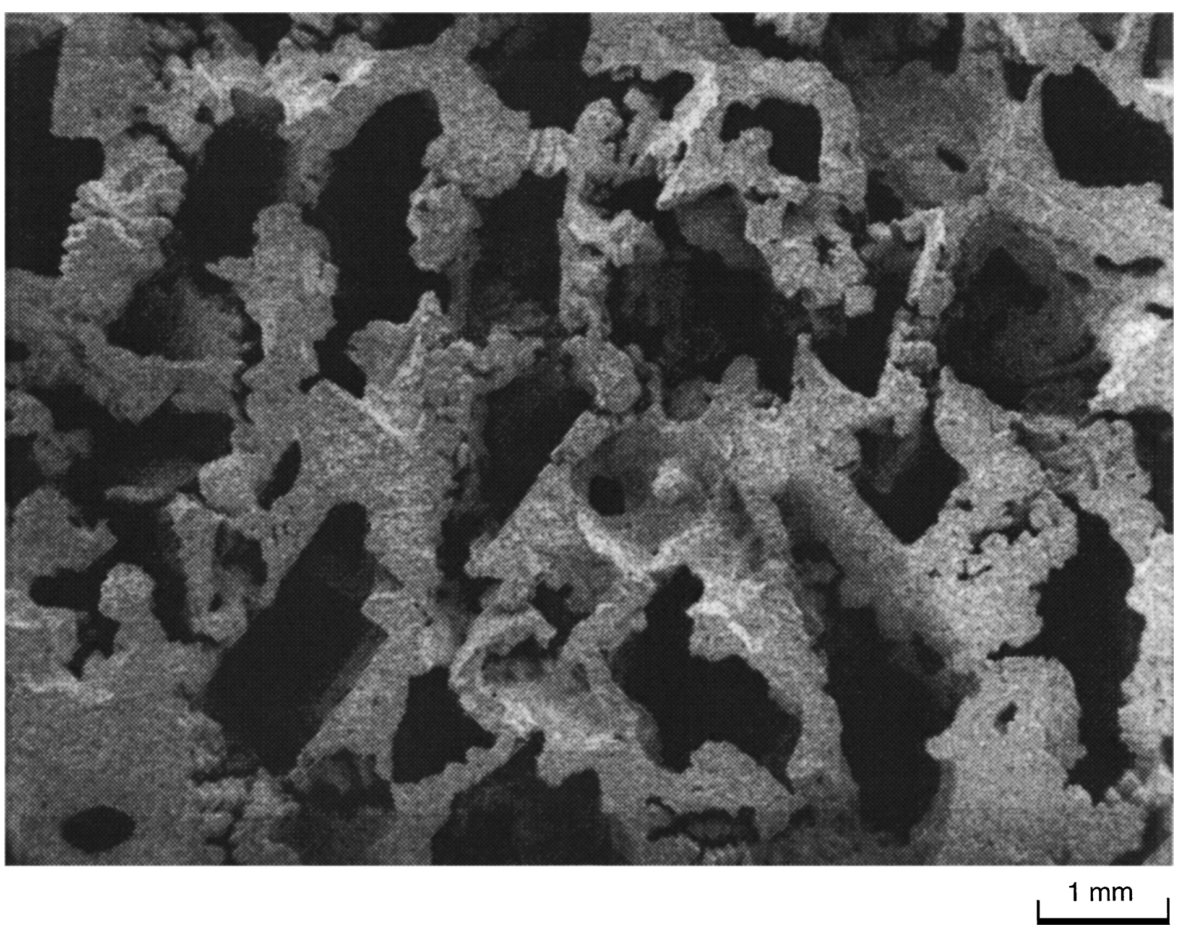

(b)

Figure 9 Microstructural features of semi-open SEU foam ($\rho = 0.35$) observed under SEM normal to (a) X_1, (b) X_2 directions.

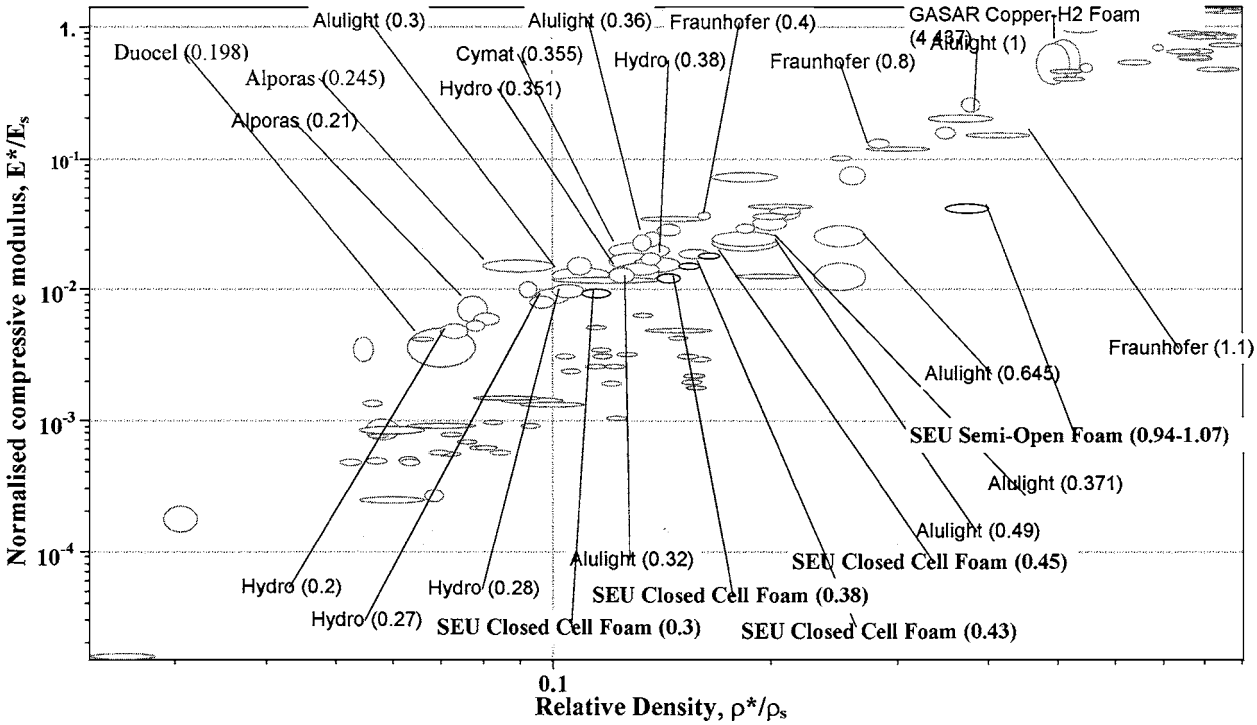

(a)

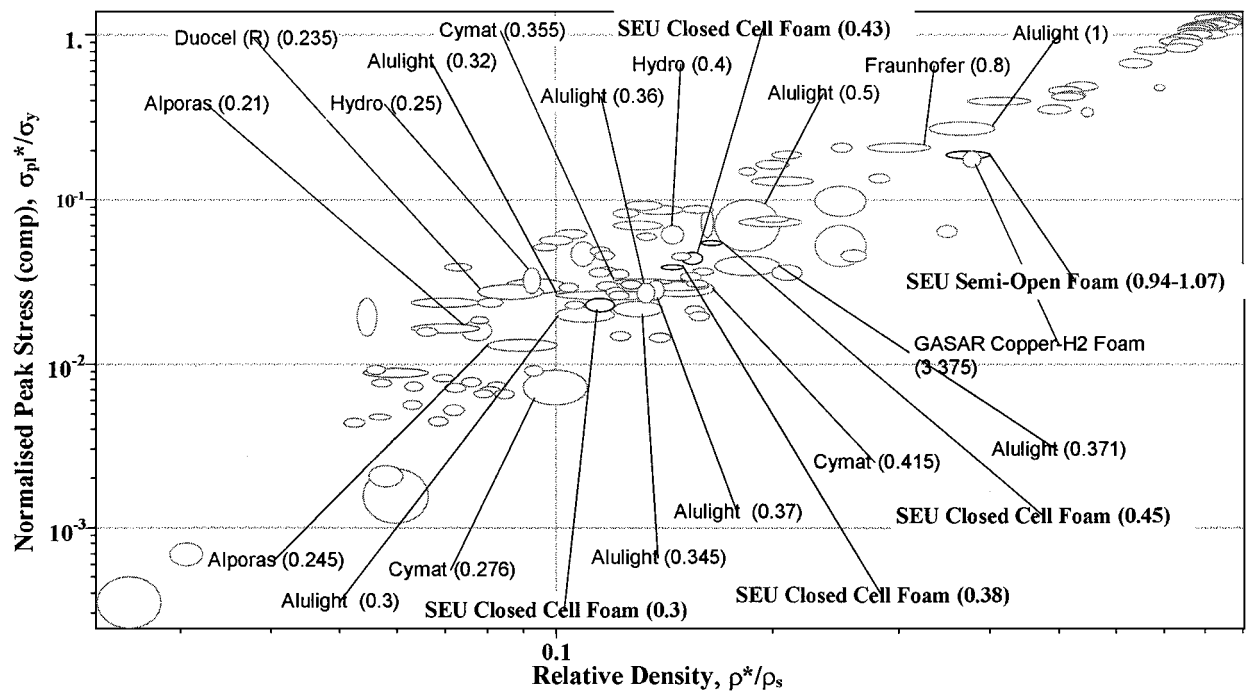

(b)

Figure 10 Cross plots of (a) Young's modulus, (b) plastic collapse strength against relative density for existing aluminium alloy foams.

5.4. Hydrostatic compression

Fig. 14 compares the hydrostatic stress versus volumetric strain curve for the SEU closed cell foam of relative density 0.14, with the uniaxial compressive stress versus strain curve of the same foam. As was previously discussed, the volumetric strain is three times the axial strain. Similar to the uniaxial compressive behaviour, the hydrostatic pressure versus volumetric strain curve has three distinct stages. During the initial linear stage where the pressure varies linearly with volumetric strain, the deformation is mainly due to the bending of cell walls. The intermediate region is characterised by a small slope (weak strain hardening) and is associated with the plastic buckling of the cell walls. Finally, when the cell walls start to make contact with each other, the slope of the curve increases and densification begins.

The stress at 10% axial strain is defined as the uniaxial compressive yield strength; similarly, in the case of hydrostatic loading, the hydrostatic pressure at 10% axial strain is defined as the hydrostatic yield strength. The measured hydrostatic yield pressure (3.2 MPa) is

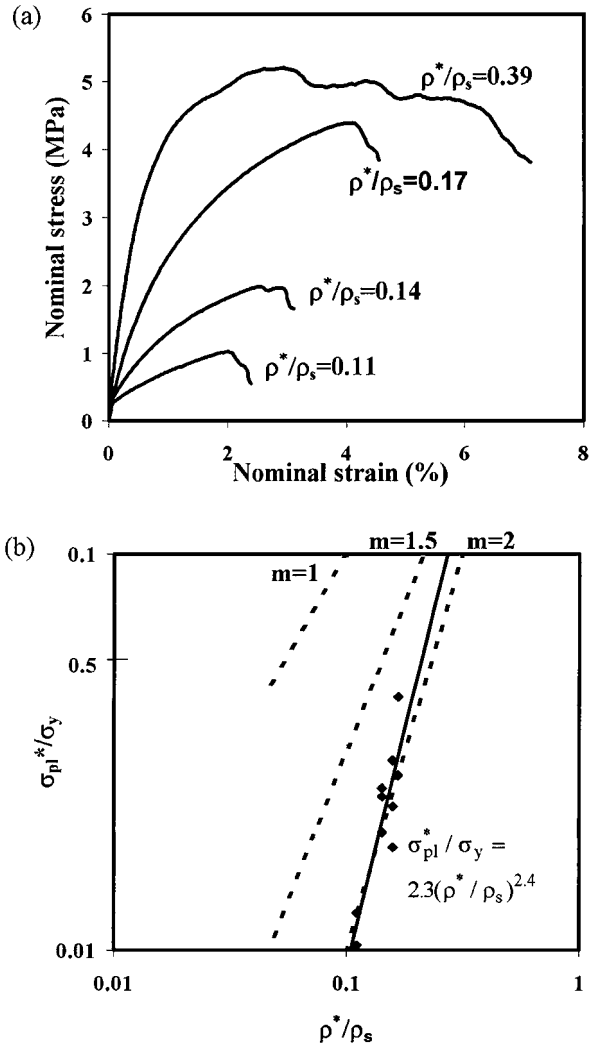

Figure 11 (a) Uniaxial tensile stress versus strain curves for SEU foams of different relative densities, (b) uniaxial tensile strength of SEU closed cell foams plotted as a function of relative density, with the dotted lines representing predictions of Equation 2, and the full line as a best fit for experimental results. Here, σ^*_{pl} is defined as the peak stress on the uniaxial tensile stress-strain curve.

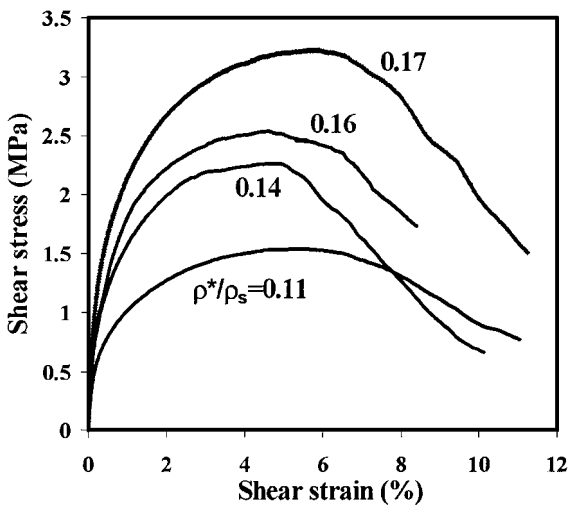

Figure 12 Shear stress versus shear strain curves for closed cell SEU foams of different relative densities.

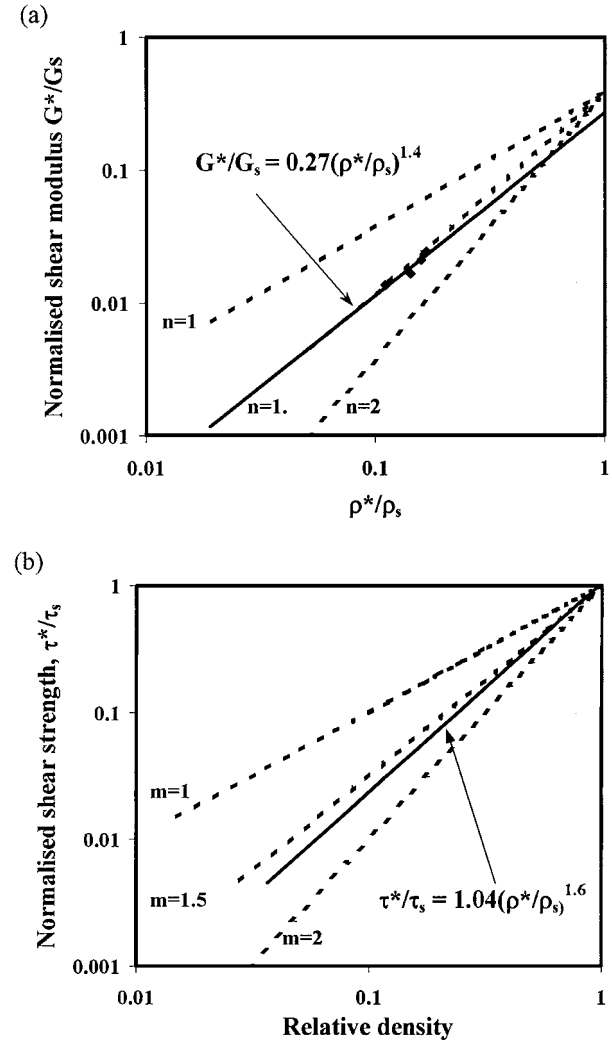

Figure 13 Cross plots of (a) Shear modulus, (b) shear strength against relative foam density for closed cell SEU foams, with the dotted lines representing predictions of Equation 4 and the full line as a best fit. Here, τ^*_{pl} is defined as the peak stress on the shear stress-strain curve.

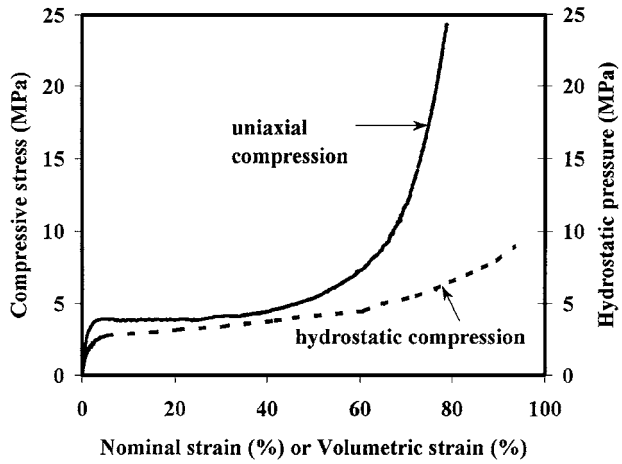

Figure 14 Hydrostatic pressure versus volumetric strain curve of SEU closed cell foam ($\rho = 0.14$) compared to the uniaxial compressive stress versus strain curve.

comparable with the uniaxial yield strength in compression (3.8 MPa), suggesting that cell wall bending, rather than cell wall stretching, dominates the deformation and failure under hydrostatic loading. Bending under hydrostatic loading is a result of imperfections in the foam structure. These include features such as cell wall curvature, local inhomogeneities (in relative density, shape or orientation), random cell structure and missing cell walls [10, 11].

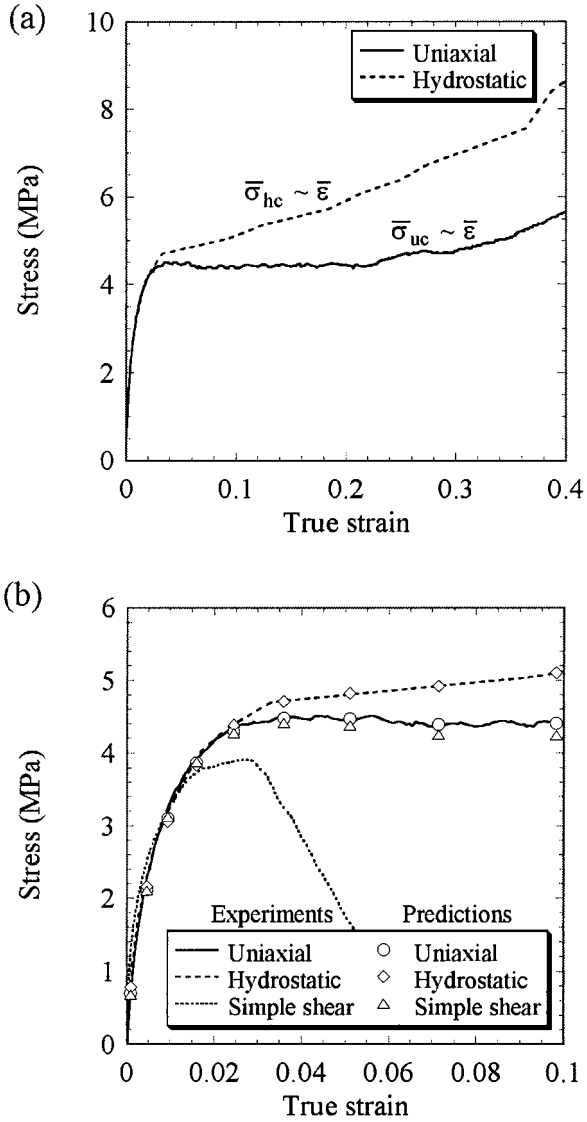

Figure 15 (a) Characteristic stress versus stain curves, (b) comparison between model predictions and experimental measurements for closed cell foam ($\rho = 0.14$) subjected to uniaxial compression, hydrostatic compression, and simple shear.

5.5. Constitutive model: Comparison with measurements

To check the validity of the constitutive model described in Section 2.2, the uniaxial compression, simple shear and hydrostatic compression results of a SEU closed cell foam ($\rho = 0.14$) are analysed. Notice that, under uniaxial, hydrostatic, or simple shear loading, Equations 11 and 12 can be simplified as

uniaxial loading

$$\bar{\sigma}_{uc} = \sqrt{1 + \beta^2/9}|\sigma|, \quad \bar{\varepsilon} = |\varepsilon|/\sqrt{1 + \beta^2/9} \tag{23}$$

hydrostatic loading

$$\bar{\sigma}_{uc} = \beta|\sigma_m|, \quad \bar{\varepsilon} = |\varepsilon_v|/\beta \tag{24}$$

simple shear

$$\bar{\sigma}_{sh} = \sqrt{3}|\tau|, \quad \bar{\varepsilon} = |\gamma|/\sqrt{3} \tag{25}$$

where the subscripts 'uc', 'hc', and 'sh' refer to uniaxial compression, hydrostatic compression, and simple shear, and τ and γ are the shear stress and engineering shear strain, respectively. The measured uniaxial stress versus strain curve and mean stress versus volumetric strain curve of the foam ($\rho = 0.14$) have been plotted in Fig. 14. These curves are then transformed into the characteristic stress versus strain curves in accordance with Equations 23 and 24, as shown in Fig. 15a. To fully determine the two material parameters $C(\bar{\varepsilon})$ and $Y(\bar{\varepsilon})$ in the yield function (15), we also need the value of β. Since the measured Young's modulus E^* and bulk modulus K^* of the foam are 0.785 GPa and 0.364 GPa, respectively, and that the Poisson ratio v^* of the foam is related to E^* and K^* by

$$v^* = \frac{1 - E^*/3K^*}{2} \tag{26}$$

one gets $v^* = 0.141$. Substitution of v^* into Equation 13 gives $\beta = 1.68$. It is noticed that since the error in measuring the mechanical properties of SEU foams is estimated to be about 10–15%, the error is also carried to the numbers quoted above.

The characteristic stress versus strain curves shown in Fig. 15a and $\beta = 1.68$ are sufficient to determine $C(\bar{\varepsilon})$ and $Y(\bar{\varepsilon})$, and hence the constitutive model is now fully specified. It may be used to predict the stress-strain relationship of the closed cell foam ($\rho = 0.14$) subjected to an arbitrary loading path. Consider the deformation behaviour of the foam under simple shear. The measured shear stress versus engineering shear strain curve is shown in Fig. 12, and is replotted using Equation 25 in Fig. 15b in terms of the characteristic stress $\bar{\sigma}_{sh}$ and strain $\bar{\varepsilon}$; the predicted $\bar{\sigma}_{sh}$ versus $\bar{\varepsilon}$ curve is included in Fig. 15b. Comparison between the model predictions and the experimental measurements for stress versus strain curves under uniaxial and hydrostatic compression is also shown in Fig. 15b. Because uniaxial compression and hydrostatic pressure are used as the characteristic tests to specify the constitutive model, it is not surprising to see from Fig. 15b that the predicted uniaxial and hydrostatic behaviours both agree well with the measurements. For the case of simple shear, the agreement is good up to the ultimate failure strength before the occurrence of softening. However, given that the failure of the foam under simple shear is by cracking rather than by plastic yielding, the present constitutive model based on the phenomenological yield function is not able to capture the fracturing behaviour of metal foams. To model the cracking induced softening, a damage model embedded in the present framework is recommended; a nonlocal approach is perhaps also needed to remedy the mathematical ill-posedness of the local approaches in the presence of softening [17, 18].

6. Conclusions

The deformation behaviours of SEU semi-open cell and closed cell foams subjected to uniaxial tension, uniaxial compression, simple shear and hydrostatic pressure are studied. The measured stiffness and strength as

functions of relative foam density are compared to those predicted from the Gibson-Ashby model. Overall, close agreement between measurements and predictions are obtained; however, the scatter of uniaxial tensile results is consistently higher than that of uniaxial compressive data. This is due to the fact that tensile testing is more prone to the effects of morphological imperfections such as fractured cell walls and holes/inclusions. The tests also reveal that the closed cell foams behave in an isotropic manner whilst the semi-open cell foams are strongly anisotropic. When loaded in the direction perpendicular to the foaming direction, X_1, the semi-open cell foams deform in a way similar to the closed cell foams where deformation bands are formed normal to the direction of applied load; the foam continues to deform until densification. When loaded in the foaming direction, X_2, shear bands are formed before crumbling failure occurs at relatively small strain levels. This is consistent with SEM images showing rounded cell cross sections in the X_1 plane and elongated elliptical cell shapes in the X_2 plane.

When the SEU closed cell foams are subjected to hydrostatic compression, it is found that the deformation consists of three different stages similar to those observed during uniaxial compression, with initial elastic deformation followed by plastic collapse and ending with a steep rise in pressure due to densification. Due to the presence of imperfections in the foam, the hydrostatic yield pressure is comparable with the uniaxial compressive strength, and is governed by cell wall bending instead of cell wall stretching expected for a perfect cellular structure such as the hexagonal honeycombs.

The measured stress versus strain curves from uniaxial compression and hydrostatic pressure are used to characterize the phenomenological constitutive model which is subsequently used to predict the deformation behavior under simple shear. The prediction agrees well with the experimental measurements until cracking (and hence softening) starts to occur in the material. More experiments need to be performed to check the applicability of the constitutive model to other loading paths including non-proportional loading. The model also needs to be improved to account for cracking and softening mechanisms.

Acknowledgement

TJL wishes to thank the financial support provided by the EPSRC (U.K.) and by the DARPA/ONR (U.S.A.) MURI program on ultralight metal structures. The authors also wish to thank Profs. D.-P. He and F. Chen of Southeast University, China, for their assistance in preparing the foam samples used in this study, and Dr. C. Chen of Cambridge University for help in constitutive modeling.

References

1. L. J. GIBSON and M. F. ASHBY, "Cellular Solids: Structure and Properties," 2nd ed. (Cambridge University Press, Cambridge, UK, 1997).
2. M. F. ASHBY, A. G. EVANS, J. W. HUTCHINSON and N. A. FLECK, "Metal Foams: A Design Guide" (Cambridge University, Engineering Department, Cambridge, UK, 1999).
3. A. G. EVANS, J. W. HUTCHINSON and M. F. ASHBY, "Current Opinion: Metals and Alloys" (1998) p. 288.
4. T. J. LU, H. A. STONE and M. F. ASHBY, *Acta Mater.* **46** (1998) 3619.
5. T. J. LU and C. CHEN, *ibid.* **47** (1999) 1469.
6. T. J. LU, A. HESS and M. F. ASHBY, *J. Appl. Phys.* **85**(11) (1999) 7528.
7. X. WANG and T. J. LU, *J. Acous. Soc. Am.* **106**(2) (1999) 756.
8. H. P. DEGISCHER, *Materials and Design* **18**(4/6) (1997) 221.
9. C. CHEN and T. J. LU, *Int. J. Solids Struc.* **37** (2000) 7769.
10. C. CHEN, T. J. LU and N. A. FLECK, *J. Mech. Phys. Solids* **47** (1999) 2235.
11. V. S. DESHPANDE and N. A. FLECK, *J. Mech. Phys. Solids*, in press.
12. L. J. GIBSON, M. F. ASHBY, J. ZHANG and T. C. TRIANTAFILLOU, *Int. J. Mech. Sci.* **31** (1989) 635.
13. M. A. PUSO and S. GOVINDJEE, *ASME MD* **68** (1995) 159.
14. J. ZHANG, Z. LIN, A. WONG, N. KIKUCHI, V. C. LI, A. F. YEE and G. S. NUSHOLTZ, *J. Engng. Mater. Tech.* **119** (1997) 284.
15. Y. SUGIMURA, J. MEYER, M. Y. HE, H. BART-SMITH, J. GRENESTEDT and A. G. EVANS, *Acta Mater.* **45** (1997) 5245.
16. K. Y. G. MCCULLOUGH, N. A. FLECK and M. F. ASHBY, *Acta Mater.* **47** (1999) 2323.
17. H. L. SCHREYER and Z. CHEN, *ASME J. Appl. Mech.* **53** (1986) 791.
18. R. H. J. PEERLINGS, R. DE BORST, W. A. M. BREKELMANS, J. H. P. DE VREE and I. SPEE, *Eur. J. Mech. A/Solids* **15** (1996) 937.

Received 14 March
and accepted 20 December 2000